Agr. Nat. Resour. 58 (2024) 321–330

AGRICULTURE AND NATURAL RESOURCES

Journal homepage: http://anres.kasetsart.org

Research article

Diethylphosphonate-containing aminoacyl-adenosine analog as inhibitor of bacterial tRNA-dependent transamidase

Withsakorn Sangsuwan[a], Anon Boonkerd[a], Chawarat Isarangkool Na Ayutthaya[a], Chanat Aonbangkhen[b], Pitak Chuawong[a,*]

[a] *Department of Chemistry and Center of Excellence for Innovation in Chemistry, Faculty of Science, Special Research Unit for Advanced Magnetic Resonance (AMR), Kasetsart University, Bangkok 10900, Thailand*

[b] *Department of Chemistry and Center of Excellence in Natural Products Chemistry (CENP), Faculty of Science, Chulalongkorn University, Bangkok 10330, Thailand*

Article Info

Article history:
Received 7 November 2023
Revised 17 November 2023
Accepted 20 November 2023
Available online 26 June 2024

Keywords:
Aminoacyl-adenosine,
Antibacterial,
Diethylphosphonate,
Transamidase

Abstract

Importance of the work: The inhibitory activity of a transition state mimic of a bacterial tRNA-dependent transamidase could help in the control of many bacterial pathogens.

Objectives: To design, synthesize and test the inhibitory activity of a transition state mimic of a bacterial tRNA-dependent transamidase.

Materials & Methods: An aminoacyl-adenosine analog was synthesized and evaluated for its inhibitory activity against GatCAB, a tRNA-dependent transamidase. The saturation transfer difference nuclear magnetic resonance (STD NMR) experiments revealed binding epitopes. The disc diffusion method was conducted to test antibacterial properties, with molecular docking simulations elucidating the binding mode of the compound.

Results: Compound 1, a non-hydrolyzable aminoacyl-adenosine analog featuring the sulfone and diethylphosphonate groups, was synthesized from 3'-deoxy-3'-aminoadenosine and NHCbz-l-cysteine. The synthesized compound retarded the transamidation rate of GatCAB by approximately 30%. In addition, the STD NMR analysis indicated binding epitopes of compound 1, highlighting interactions involving the hydrogens in the diethylphosphonate, anomeric position and the adenine ring. Molecular docking simulations further elucidated the binding mode of compound 1 at the GatB transamidation site. Nonetheless, compound 1 did not exhibit *in vivo* antibacterial effects against *Pseudomonas aeruginosa*, *Staphylococcus aureus* or *Bacillus subtilis*, presumably due to cell permeability issues.

Main finding: The inhibition was highlighted of the tRNA-dependent transamidase, a novel target for antimicrobial development. Further structural modification to enhance membrane permeation could provide an antibacterial agent with a novel mechanism of action.

* Corresponding author.
E-mail address: Pitak.C@ku.ac.th (P. Chuawong)

https://doi.org/10.34044/j.anres.2024.58.3.05

Introduction

Antimicrobial resistance (AMR) is an imminent public health problem worldwide with multidrug resistance (MDR) infections leading to hospital morbidity and mortality (Agyeman et al., 2022). Furthermore, progress in developing novel antibacterial agents with innovative mechanisms of action has been notably sluggish compared to the increasing emergence of new antimicrobial resistance (Vila et al., 2020). Therefore, efforts into antibacterial drug discovery are ongoing. Despite the discoveries of various natural products with antimicrobial activities (Khuntong, 2008; Rossiter et al., 2017; Namsena et al., 2019; Elmaidomy et al., 2022; Sae-lim et al., 2023), the abovementioned medical challenges have prompted the current investigation of novel targets for the development of antibacterial drugs. Several biochemical processes, such as cell wall biosynthesis, fatty acid biosynthesis, and protein biosynthesis, have been exploited as antibacterial drug targets (Belete, 2019). Specifically, ribosomal protein biosynthesis or translation presents an appealing target due to its important distinctions from the human counterpart (Lin et al., 2018). One of the key players in maintaining translational fidelity is the enzyme aminoacyl-tRNA synthetase, which covalently links an amino acid with its cognate tRNA isoacceptors that are subsequently loaded onto the ribosome for peptide bond formation (Ibba and Söll, 2000).

It was hypothesized that there should be 20 aminoacyl-tRNA synthetases, one for each pair of amino acids and tRNA isoacceptors. However, all archaea and many pathogenic bacteria lack genes encoding some of the aminoacyl-tRNA synthetases, in particular, those for glutaminyl-tRNA synthetase (GlnRS) and asparaginyl-tRNA synthetase (AsnRS) (Woese et al., 2000). These organisms rely on indirect tRNA aminoacylation to establish a complete set of aminoacyl-tRNAs for protein biosynthesis (Cathopoulis et al., 2007). First, $tRNA^{Gln}$ and/or $tRNA^{Asn}$ are charged with glutamate and aspartate to generate Asp-$tRNA^{Asn}$ and/or Glu-$tRNA^{Gln}$ by the non-discriminating tRNA synthetases (Rathnayake et al., 2017). Then, these incorrectly charged tRNAs are converted to Asn-$tRNA^{Asn}$ and/or Gln-$tRNA^{Gln}$ via the transamidation process, which involves the conversion of the carboxylate side chain to its carboxamide by the Asp-$tRNA^{Asn}$/Glu-$tRNA^{Gln}$ amidotransferase (GatCAB) (Curnow et al., 1997). GatCAB is a heterotrimeric enzyme catalyzing a three-step process, as illustrated in Scheme 1. First, GatA hydrolyzes glutamine to provide ammonia (Reaction 1), which is used in the subsequent step. Then, GatB phosphorylates the carboxylate side chain of the mischarged tRNA (Reaction 2). Finally, the ammonia generated by GatA travels through a hydrophilic tunnel (Zhao et al., 2012; Zhao et al., 2016) to GatB and attacks the carbonyl group of the phosphorylated carboxylic group to yield an amide (Reaction 3). Notably, GatC does not contribute to the catalytic activity of GatCAB but has a presumed structural role.

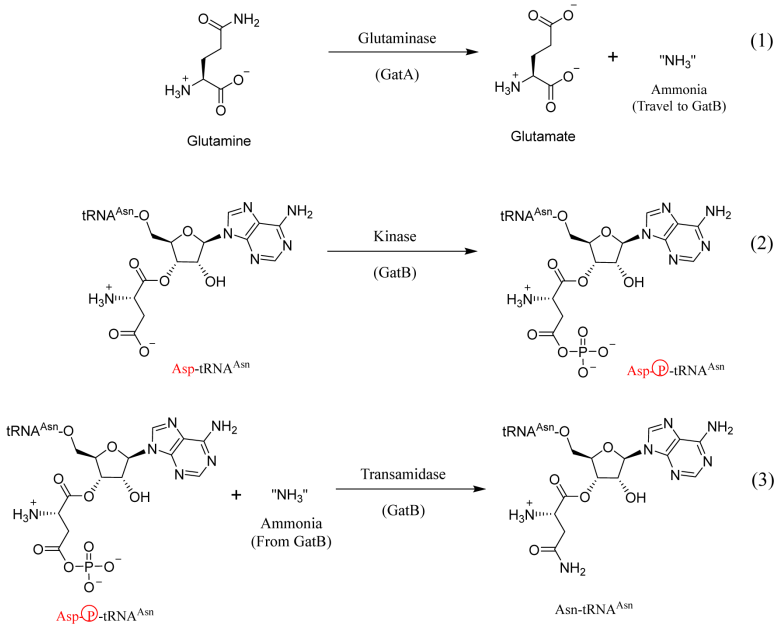

Scheme 1 tRNA-dependent transamidation catalyzed by GatCAB

GatCAB has been explored as an antibacterial target due to its indispensability in many human pathogens and the absence of a human homolog (Pham and Lapointe, 2017). The most effective inhibitor thus far is the puromycin analog bearing methylsulfone on the amino acid moiety reported by Balg et al. (2008), as illustrated in Fig. 1. This inhibitor mimics the tetrahedral transition state of the transamidation reaction (Reaction 3 in Scheme 1). Notably, puromycin is a non-selective antibiotic with high systemic toxicity (Aviner, 2020) and therefore, it has never made it to clinical trials. Consequently, searching for a new puromycin analog that confers more desirable pharmacological properties is of much interest.

Inspired by the most potent inhibitor reported by Balg et al. (2008), the current study designed a new transamidase inhibitor containing a diethylphosphonate group adjacent to the methylsulfone, compound 1 (Fig. 1). The diethylphosphonate was incorporated into the structure to mimic the phosphate group on the transamidation substrate. Notably, the removal of the diethyl group would render the inhibitor more analogous to the transamidation substrate. However, at physiological pH, the phosphate group is completely ionized, providing two negatively charged oxygen atoms that make the molecule extremely hydrophilic and, therefore, reduce protein binding capability. Therefore, the neutral diethylphosphonate group was expected to ease hydrophilicity and promote binding to GatB.

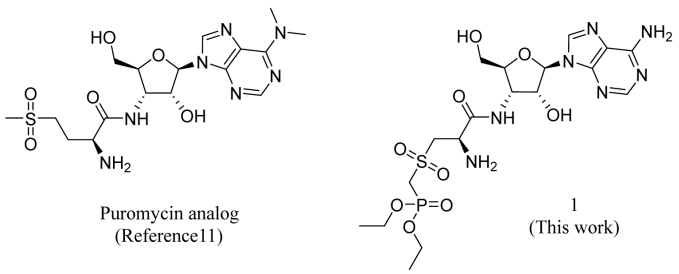

Fig. 1 Puromycin analog and compound 1 as inhibitors of GatCAB

Materials and Methods

General methods

Starting materials and reagents were obtained from commercial sources and used without additional purification. The reactions were monitored based on thin-layer chromatography (TLC) using TLC silica gel 60, F254 plates from Merck. The reaction mixtures were purified using flash column chromatography and SiliCycle SiliaFlash® F60, 40–63 µm (230–400 mesh). ^{1}H and ^{13}C NMR spectra were recorded on a Bruker Avance NanoBay 400 MHz spectrometer. High-resolution mass spectra (HRMS) were obtained using a Bruker Daltonics microTOF instrument operating in electrospray positive ionization mode. Melting points (mp) were determined using the Stuart SMP10 apparatus without corrections.

Synthesis

(Diethoxyphosphoryl)methyl methanesulfonate (3) was synthesized using the following procedure (Romeo et al., 2012). To a cooled solution of diethyl (hydroxymethyl) phosphonate (compound 2, 1.13 g, 6.70 mmol) in 60 mL anhydrous CH_2Cl_2 was added Et_3N (2.8 mL, 20 mmol) and MsCl (0.7 mL, 9 mmol). The reaction mixture was stirred for 1 hr. A saturated NH_4Cl solution was added and the mixture was extracted thrice using CH_2Cl_2. The combined organic layers were dried over anhydrous Na_2SO_4 and concentrated under reduced pressure. The residue was purified using flash column chromatography (60−100% EtOAc/pentane) to give compound 3 (1.19 g, 72%) as a yellow oil. ^{1}H NMR (400 MHz, $CDCl_3$) δ 4.39 (d, J = 8.9 Hz, 2H), 4.20 (dq, J = 8.5, 7.1 Hz, 4H), 3.11 (s, 3H), 1.35 (t, J = 7.1 Hz, 6H); ^{13}C NMR (100 MHz, $CDCl_3$) δ 63.51 (d, J = 6.4 Hz), 61.22 (d, J = 169.5 Hz), 38.02, 16.48 (d, J = 5.7 Hz); HRMS (ESI-TOF), *m/z* calcd for $C_6H_{15}NaO_6PS$ $[M+Na]^+$ 269.0219, found 269.0221.

((Benzyloxy)carbonyl)(((diethoxyphosphoryl)methyl) sulfonyl)-D-alanine (4) was synthesized as follows. A cooled mixture of NHCbz-l-cysteine (836 mg, 3.28 mmol) and K_2CO_3 (1.4 g, 10 mmol) in CH_3CN (16 mL) was bubbled with Ar for 5 min. Then, the solution of compound 3 (1.21 g, 4.91 mmol) in CH_3CN (16 mL) was added and the reaction mixture was stirred at room temperature for 16 hr under an Ar atmosphere. After removal of the solvent under reduced pressure without heating, the residue was dissolved in cooled 0.1 M NaOH and washed with CH_2Cl_2 to remove the unreacted mesylate. The pH of the solution was adjusted to 1 using 6 M HCl. The mixture was extracted thrice with EtOAc and the combined organic layers were dried over anhydrous Na_2SO_4 and concentrated to obtain a yellow oil, which was used in the next step without further purification.

To a cooled solution of the yellow oil in 30 mL MeOH was added, dropwise, the solution of Oxone® (3 g, 9 mmol) in H_2O (30 mL). The reaction mixture was stirred at room temperature for 6 hr. Then, the MeOH was removed under reduced pressure without heating and the residue was extracted thrice with EtOAc. The combined organic layers were dried over anhydrous Na_2SO_4 and concentrated to give compound 4 (1.31 g, 91%) as a white solid. mp = 130−132 °C; ^{1}H NMR (400 MHz, $CDCl_3$) δ 7.75 (br s, 1H), 7.36–7.27 (m, 5H), 6.32 (d, J = 8.4 Hz, 1H), 5.16 (d, J = 12.2 Hz, 1H), 5.09 (d, J = 12.5 Hz, 1H), 4.91–4.84 (m, 1H), 4.29–4.08 (m, 4H), 3.93–3.78 (m, 3H), 3.75–3.63 (m, 1H), 1.34 (t, J = 7.1 Hz, 3H), 1.28 (t, J = 7.1 Hz, 3H); ^{13}C NMR (100 MHz, $CDCl_3$) δ 171.3, 156.4, 136.1, 128.6, 128.3, 128.1, 67.5, 64.8 (d, J = 6.6 Hz), 64.4 (d, J = 6.5 Hz), 55.9, 51.9 (d, J = 139.4 Hz), 50.1, 16.3 (d, J = 4.1 Hz), 16.3 (d, J = 4.1 Hz); HRMS (ESI-TOF), *m/z* calcd for $C_{16}H_{24}NNaO_9PS$ $[M+Na]^+$ 460.0802, found 460.0831.

Benzyl ((*R*)-1-(((2*S*,3*R*,4*R*,5*R*)-5-(6-amino-9*H*-purin-9-yl)-4-((*tert*-butyldimethylsilyl)oxy)-2-(((*tert*-butyldimethylsilyl)oxy)methyl)tetrahydrofuran-3-yl)amino)-3-(((diethoxyphosphoryl)methyl)sulfonyl)-1-oxopropan-2-yl) carbamate (5) was synthesized as follows. To a cooled solution of 9-((2*R*,3*R*,4*R*,5*S*)-4-amino-3-((*tert*-butyldimethylsilyl) oxy)-5-(((*tert*-butyldimethylsilyl)oxy)methyl)tetrahydrofuran-2-yl)-9*H*-purin-6-amine (Klinchan et al., 2014) (260 mg, 0.525 mmol) and compound 4 (344 mg, 0.786 mmol) in anhydrous CH_2Cl_2 (10 mL) was added EDC•HCl (121 mg, 0.631 mmol). The reaction mixture was degassed and filled with Ar before stirring at room temperature for 16 hr. Then, water was added and the solvents were removed under reduced pressure without heating. Subsequently, EtOAc and water were added and the solution was sequentially washed with 5% citric acid, water, saturated $NaHCO_3$ and brine. The organic layer was collected, dried over anhydrous Na_2SO_4, and concentrated under reduced pressure to give the crude mixtures, which were purified using flash column chromatography (4% MeOH/CH_2Cl_2) to give compound 5 (424 mg, 88%) as a white solid. mp = 74−80 °C; ^{1}H NMR (400 MHz, $CDCl_3$) δ 8.34 (s, 1H), 8.31 (s, 1H), 7.40–7.28 (m, 6H), 6.16 (d, J = 8.4 Hz, 1H), 6.06 (d, J = 2.5 Hz, 1H), 5.73 (s, 2H), 5.13 (s, 2H), 4.97–4.87 (m, 1H), 4.65–4.56 (m, 2H), 4.27–4.14 (m, 5H), 4.08–3.94 (m, 2H), 3.91–3.72 (m, 3H), 3.65 (dd, J = 15.0, 4.4 Hz, 1H), 1.39–1.30 (m, 6H), 0.95 (s, 9H), 0.84 (s, 9H), 0.13 (s, 6H), 0.06 (s, 3H), 0.01 (s, 3H); ^{13}C NMR (100 MHz, $CDCl_3$) δ 168.6, 156.3, 155.5, 153.1, 149.8, 139.0, 135.9 (d, J = 1.8 Hz), 128.7, 128.5, 128.3, 120.0, 89.7, 83.7, 76.2, 67.7, 64.1 (d, J = 7.0 Hz), 64.0 (d, J = 6.6 Hz), 62.4, 57.5, 51.5 (d, J = 136.8 Hz), 50.9, 26.2, 25.8, 18.7, 18.0, 16.4 (d, J = 5.5 Hz), –4.8, –5.0, –5.2, –5.3; HRMS (ESI-TOF), *m/z* calcd for $C_{38}H_{65}N_7O_{11}PSSi_2$ $[M+H]^+$ 914.3733, found 914.3696.

Diethyl ((((*R*)-2-amino-3-(((2*S*,3*R*,4*R*,5*R*)-5-(6-amino-9*H*-purin-9-yl)-4-((*tert*-butyldimethylsilyl)oxy)-2-(((*tert*-butyldimethylsilyl)oxy)methyl)tetrahydrofuran-3-yl)amino)-3-oxopropyl)sulfonyl)methyl)phosphonate (6) was synthesized as follows. To a solution of compound 5 (270 mg, 0.295 mmol) in MeOH (6 mL) containing 1% AcOH was added 10% Pd/C (63 mg, 59 µmol). The reaction mixture was stirred at room temperature under an H_2 atmosphere for 1 hr. Then, the catalyst was removed using filtration through a short pad of Celite® and the filtrate was added to a saturated $NaHCO_3$ solution before being concentrated under reduced pressure. The residue was dissolved in water and extracted thrice with EtOAc. The combined organic layers were dried over anhydrous Na_2SO_4 and concentrated to give the crude mixtures, which were purified using flash column chromatography (4% MeOH/CH_2Cl_2) to obtain compound 6 (208 mg, 90%) as a white solid. mp = 60−70 °C; ^{1}H NMR (400 MHz, $CDCl_3$) δ 8.33 (s, 1H), 8.31 (s, 1H), 8.01 (d, J = 7.0 Hz, 1H), 6.09 (d, J = 3.4 Hz, 1H), 5.74 (s, 2H), 4.62 (dd, J = 5.6, 3.4 Hz, 1H), 4.52 (q, J = 6.3 Hz, 1H), 4.27–4.18 (m, 5H), 4.07–3.99 (m, 2H), 3.96–3.58 (m, 5H), 1.39–1.33 (m, 6H), 0.95 (s, 9H), 0.87 (s, 9H), 0.13 (s, 6H), 0.03 (s, 6H); ^{13}C NMR (100 MHz, $CDCl_3$) δ 171.8, 155.5, 153.2, 149.9, 138.9, 119.9, 89.3, 84.3, 76.4, 63.9 (d, J = 6.5 Hz), 63.1, 58.9, 52.6 (d, J = 138.3 Hz), 51.2, 51.0, 26.2, 25.8, 18.7, 18.0, 16.4 (d, J = 6.3 Hz), –4.8, –4.9, –5.2, –5.3; HRMS (ESI-TOF), *m/z* calcd for $C_{30}H_{59}N_7O_9PSSi_2$ $[M+H]^+$ 780.3366, found 780.3369.

Diethyl ((((*R*)-2-amino-3-(((2*S*,3*S*,4*R*,5*R*)-5-(6-amino-9*H*-purin-9-yl)-4-hydroxy-2-(hydroxymethyl)tetrahydrofuran-3-yl)amino)-3-oxopropyl)sulfonyl)methyl)phosphonate (1) was synthesized as follows. To a cooled solution of compound 6 (347 mg, 0.445 mmol) in anhydrous tetrahydrofuran (THF; 5 mL) was added DIPEA (0.4 mL, 2 mmol), followed by Et_3N•3HF (145 µL, 0.890 mmol). The reaction mixture was stirred at room temperature for 16 hr. After cooling to 0°C, $NaHCO_3$ (224 mg, 2.67 mmol) and water were added sequentially. The mixture was allowed to adjust to room temperature and stirred until gas bubbles ceased. Then, the THF was removed under reduced pressure without heating and the aqueous solution was washed with CH_2Cl_2. After the solvent removal, the residue was charged using a MeOH-to-CH_2Cl_2 ratio of 1:1 and the undissolved solids were removed. Then, the solution was concentrated to give the crude mixtures,

which were purified using preparative reverse-phase chromatography with a Buchi PrepPure C-850 FlashPrep liquid chromatography (LC) system with 30−40% MeOH/H_2O to produce compound 1 (75 mg, 30%) as a white solid. mp = 60−70 °C; ^{1}H NMR (400 MHz, DMSO-d_6) δ 8.41 (s, 1H), 8.29 (d, J = 6.8 Hz, 1H), 8.16 (s, 1H), 7.32 (s, 1H), 6.09 (s, 1H), 5.97 (d, J = 3.2 Hz, 1H), 5.20 (t, J = 5.6 Hz, 1H), 4.59–4.27 (m, 4H), 4.15–4.00 (m, 5H), 3.89–3.80 (m, 1H), 3.76–3.66 (m, 1H), 3.60–3.47 (m, 3H), 2.19 (s, 2H), 1.25 (t, J = 7.0 Hz, 6H); ^{13}C NMR (100 MHz, DMSO-d_6) δ 172.7, 156.2, 152.7, 148.9, 139.3, 119.2, 89.4, 83.4, 73.2, 62.8 (d, J = 6.2 Hz), 62.6 (d, J = 6.1 Hz), 61.1, 58.2, 50.7, 50.6 (d, J = 133.7 Hz), 50.6, 16.2 (d, J = 6.2 Hz); HRMS (ESI-TOF), *m/z* calcd for $C_{18}H_{30}N_7NaO_9PS$ $[M+Na]^+$ 574.1456, found 574.1436.

The percentage purity of compound 1 was determined using a Shimadzu high-performance liquid chromatography (HPLC) system equipped with a Kaseisorb LC column (ODS 2000, C-18, 4.6×250 mm). See Fig. S42 for the chromatogram.

Transamidase assays

The GatCAB transamidase assay was conducted following the condition reported by Lapoint and co-workers (Balg et al., 2008). GatCAB was overexpressed and purified from *E. coli* BL21(DE3) harboring plasmids pSS003 (N-terminal 6-His GatB) and pPTC032 (N-terminal 6-His GatC), according to the protocol published by Zhao et al. (2012). The Asp-tRNA^{Asn} was prepared from an aspartylation reaction catalyzed by *H. pylori* non-discriminating aspartyl-tRNA synthetase with tRNA^{Asn} overtranscribed and purified from *E. coli* (MV1184) harboring plasmid pPTC011, according to the protocol reported by Zhao et al. (2016). The assay mixture consisted of 50 mM HEPES.KOH pH 7.0, 15 mM $MgCl_2$, 25 mM KCl, 1.28 mM Gln, 1 mM DTT, 2 mM ATP, 0.5 µM Asp-tRNA^{Asn} and 12 nM GatCAB in the absence or presence of compound 1 (2 mM). The 20 s interval aliquots (40 µL each) were removed from the reaction and quenched with cooled 40% volume per volume of 0.6 M NaOAc buffer pH 5.2 in *i*-PrOH and then left at -80°C for 1 hr. After centrifugation at 20,000×*g* at 4°C for 30 min, the supernatant was carefully removed and the tRNA pellets were resuspended in 20 µL of 50 mM KOH. The deacylation was completed by heating the mixture at 65°C for 10 min. Subsequently, amino acids in the reaction mixtures were derivatized using 6-aminoquinolyl-*N*-hydroxysccinimidylcarbamate (AQC), according to Horiuchi et al. (2001). The transamidation rate of GatCAB was determined with respect to the asparagine concentration at each reaction time point, which was determined based on HPLC coupled to fluorescence detection (FLD), conducted on an Agilent 1260 Infinity II HPLC-FLD with a Poroshell 120 SB-C-18 column, 4.6×100 mm, 2.7 µm with a gradient elution of eluent A (50 mM NaOAc buffer pH 6.0 containing 5% acetonitrile) and eluent B (100% acetonitrile). The excitation and emission wavelengths for FLD were 254 and 400 nm, respectively.

Saturation transfer difference nuclear magenetic resonance experiment

Compound 1 and *H. pylori* GatB, overexpressed and purified according to the reported protocol for GatCAB (Zhao et al., 2012), were dissolved in 400 µL of 50 mM Na_2HPO_4, 100 mM NaCl, pH 7.5 in D_2O to the final concentration of 3 mM (ligand) and 30 µM (protein), respectively. The mixture was incubated at room temperature for 1 hr. Then, the saturation transfer difference nuclear magnetic resonance (STD NMR) experiment was conducted on a Bruker Avance NanoBay 400 MHz spectrometer using a conventional inverse 5 mm probe with the z-gradient at 25°C. The standard pulse program for an STD experiment (stddiffesgp) was used with a number of scans of 16 and a number of averages of 64. The saturation time (D20) and relaxation delay (D1) were set to 2.0 s. The spectra obtained from the "Off" and "On" resonances were subtracted and the STD spectrum (difference) was obtained. The STD amplification factor (STDamp) was calculated for each STD-active signal using Equation 1:

$$\text{STDamp} = \left(\frac{\text{STDdiff}}{\text{STDoff}}\right) \times \text{Ex} \quad (1)$$

where STDdiff and STDoff are the intensities of resonances from the STD difference and the reference spectra, respectively, and Ex is the ligand excess. In the current experiment, the Ex value was 100 (GatB:compound 1 = 1:100). The percentage of STD maximum signal was calculated with respect to the resonance with the strongest STD signal, which was set to 100%.

Molecular docking simulations

The three-dimensional structure of compound 1 was acquired through the DFT calculations using the M062X method with a 6-31G(d,p) basis set implemented in the Gaussian09W software (Frisch et al., 2009). The structure of GatB from *H. pylori* was obtained via template-based

modeling (I-TASSER; https://zhanggroup.org/I-TASSER/) (Yang and Zhang, 2015; Zheng et al., 2021; Zhou et al., 2022). The protein and ligand PDBQT files were prepared using the AutoDockTools 1.5.6 software (Sanner, 1999). The grid box dimensions were 20 Å × 20 Å × 20 Å, covering the transamidase active site of GatB. Molecular docking was performed using the AutoDock Vina software (Trott and Olson, 2010; Eberhardt et al., 2021), and the best-docked conformation was analyzed using the Discovery Studio Visualizer V21.1.0.20298 software (BIOVIA, 2020) and PyMol Version 2.5.5 software (Schrodinger, 2023).

Antibacterial evaluation

The antibacterial efficacy of compound 1 was assessed using a disc diffusion method. One Gram-negative bacterium, *Pseudomonas aeruginosa* ATCC 27853, and two Gram-positive bacteria, *Staphylococcus aureus* ATCC 25923 and *Bacillus subtilis* ATCC 6633, were tested. An overnight culture of each bacterium was transferred to a sterile saline solution (0.85% NaCl) and the turbidity was adjusted to match a 0.5 McFarland standard, corresponding to a concentration of 1×10^8 colony forming units/mL. The bacterial suspension was spread on the surface of Mueller Hinton agar. Subsequently, the discs (each 6 mm in diameter) were placed on the agar surface and loaded with 20 µL of the tested inhibitor solution (10 mg/mL in dimethyl sulfoxide; DMSO). After incubation at 37°C for 24 hr, the antibacterial activity was assessed by measuring the diameter of the inhibition zones. Penicillin and gentamycin were used as the positive controls for the Gram-positive and Gram-negative bacteria, respectively.

Results and Discussion

Synthesis of compound 1

Scheme 2 illustrates the synthesis of compound 1, starting from the preparation of the diethylphosphonate-containing amino acid. The hydroxyl group of compound 2 was activated via mesylation using methanesulfonyl chloride to produce compound 3 with a 72% yield. Then, the substitution reaction between compound 3 and NHCbz-L-cysteine provided the sulfide intermediate, which was subsequently oxidized using Oxone® to produce compound 4 with a 91% yield over two steps.

With the diethylphosphonate-containing amino acid in hand, the coupling reaction between compound 4 and the TBS-protected-3′-aminoadenosine, which was prepared based on our published protocol (Klinchan et al., 2014), was carried out. The coupling reaction utilizing a carbodiimide reagent went smoothly, producing compound 5 with a good yield. The Cbz protecting group was removed via hydrogenolysis using Pd/C and hydrogen gas to produce compound 6 with a 90% yield. Finally, the silyl protecting groups were removed using a neutral, nucleophilic fluorinating reagent $Et_3N{\cdot}3HF$ (Veyron et al., 1989) to produce compound 1 with a 30% yield. Notably, desilylation at this late synthetic stage with simple fluoride reagents such as NaF or n-Bu_4NF (TBAF) did not provide desirable results.

Transamidase inhibition of compound 1

The investigation of GatCAB inhibition has been reported elsewhere. For example, Decicco et al. (2001) published research on the inhibitory effects of glutamine analogs against both the glutaminase and transamidase activities of GatCAB. Additionally, inhibitory properties have been observed in ATP (Horiuchi et al., 2001), chloramphenicol (Balg et al., 2010), and 3′-end tRNA (Huot et al., 2007; Balg et al., 2008; Pham et al., 2016a) analogs against GatCAB. Furthermore, Pham et al. (2016b) reported the competitive inhibition of *H. pylori* GatCAB by cyclic peptides.

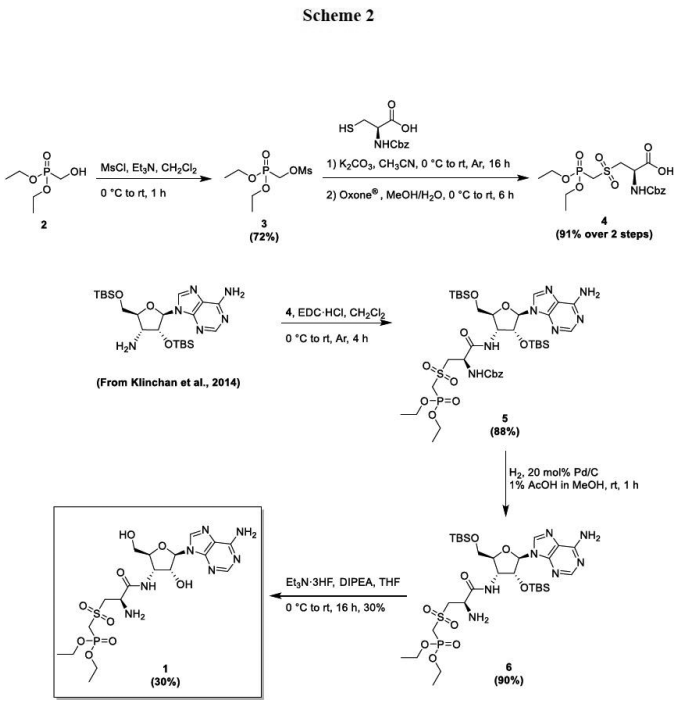

Scheme 2 Synthesis of compound 1

Herein, the transamidase activity of *H. pylori* GatCAB was monitored under the reported conditions (Balg et al., 2008). The formation of Asn-tRNA^{Asn} was directly proportional to the concentration of asparagine in the AQC-derivatized mixture, which was quantified using HPLC-FLD techniques. The reaction proceeded smoothly at a rate of 0.058 µM/min in the absence of compound 1 (See Fig. S1 for the initial rate plot). However, the transamidation rate decreased to 0.041 µM/min in the presence of 2 mM compound 1. Fig. 2 illustrates the relative rate of transamidation. Compound 1 decreased the transamidation rate by approximately 30%. Therefore, the initial kinetic inquiry revealed the inhibitory potential of the compound. Nonetheless, the comprehensive elucidation of the inhibition mechanism remains an ongoing effort, with sharing of the results of these ongoing experiments in an upcoming report.

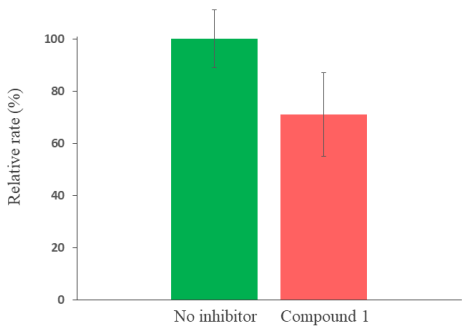

Fig. 2 Relative transamidation rate of the Glu-tRNA^{Gln}/Asp-tRNA^{Asn} amidotransferase (GatCAB) from *H. pylori*, where reactions were conducted in presence or absence of 2 mM compound 1 and error bars represent ± SD of reactions run in triplicate

Saturation transfer difference nuclear magnetic resonance spectroscopy

Epitope maps of ligand binding to a protein receptor can be illustrated qualitatively and quantitatively using the STD NMR spectroscopic technique (Meyer and Peters, 2003). Compound 1 was designed based on the transition state of the transamidation and, therefore, was expected to interact with the transamidase center in GatB. Initially, GatB was overexpressed and purified, according to the protocol of Zhao et al. (2012). Subsequently, compound 1 and GatB were incubated in a deuterated phosphate-buffered saline for 1 hr and the STD NMR spectrum was collected afterward. Fig. 3 illustrates the STD and the reference NMR spectra. Protons at the 2 (magenta) and 8 (turquoise) positions of the adenine ring showed the STD signals, implying binding of the adenine moiety to GatB, with the proton at the 2 position exhibiting the highest (100%) STD amplification among all STD-active resonances. Notably in compound 1, the proton at the 8 position exhibited the nOe correlation to the anomeric proton, distinguishing it from the other aromatic proton at the 2 position of the adenine ring (See Fig. S37 for the nuclear Overhauser effect spectrum of compound 1). The binding of the adenine ring to a protein has also been observed using the STD NMR technique. For example, Igonet et al. (2018) observed the binding of adenosine to its receptors via STD NMR. Furthermore, STD NMR facilitated fragment screening in their study. In addition, binding of the methyl (orange) and the anomeric (blue) protons to GatB was observed, as illustrated in Fig. 3.

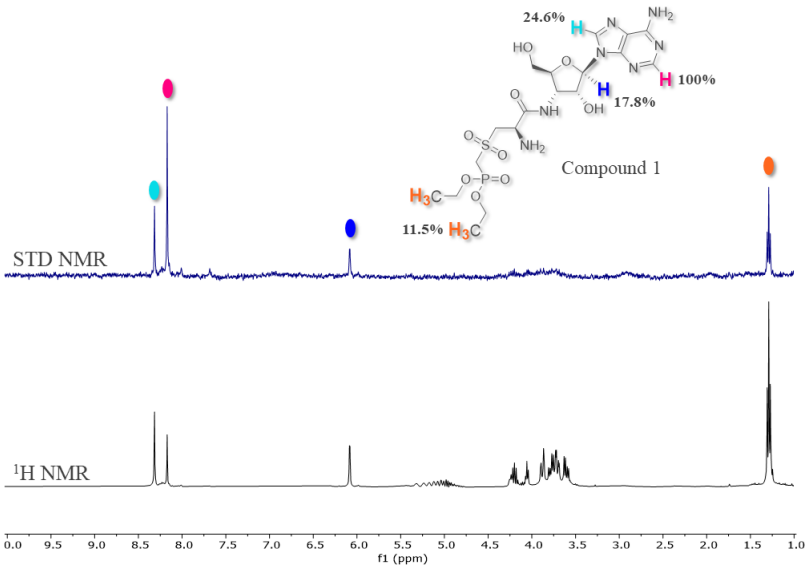

Fig. 3 Saturation transfer difference (STD) and nuclear magnetic resonance (NMR) spectra of mixture of compound 1 and GatB (protein:ligand = 1:100), with percentage of STD maximum signal displayed for each STD-active proton and ppm = parts per million

Nonetheless, STD NMR only elucidated epitope maps based on the ligand ^{1}H NMR signals and did not provide information regarding the binding site on the receptor. Therefore, the molecular docking simulations were studied to suggest the binding mode of compound 1 to GatB.

Molecular docking simulations

Several crystal structures of GatCAB have become available and have facilitated mechanism-based drug design (Nakamura et al., 2006, 2010; Wu et al., 2009; Blaise et al., 2010; Suzuki et al., 2015). However, the structure of *H. pylori* GatCAB is not available thus far. Therefore, the current study generated a three-dimensional structure of *H. pylori* GatB, the transamidase center, using I-TASSER (iterative threading assembly refinement) protein structure prediction tool, available online (Yang and Zhang, 2015; Zheng et al., 2021; Zhou et al., 2022). The structure was acquired using iterative template-based fragment assembly simulations. Then, the DFT calculations were conducted to obtain a three-dimensional structure of compound 1. Molecular docking simulations with AutoDock Vina suggested the binding mode of compound 1 to *H. pylori* GatB. Fig. 4 illustrates key interactions between *H. pylori* GatB and compound 1 (See all binding interactions in Fig. S5). Lys80 and Tyr271 formed hydrogen bonds with the oxygen atoms of the diethylphosphonate moiety of compound 1. Tyr273 interacted with the oxygen atom of the sulfone and the amino group via hydrogen bonding. In addition, Glu211 and Ser154 formed hydrogen bonds to the 2′-hydroxyl group of the ribose and the amino group of the adenine base, respectively. The π-cation interactions were established between the adenine and Arg209. Notably, the transamidation active site of GatB was relatively exposed, rendering high solvent accessibility and, presumably, facilitating the binding of relatively hydrophilic molecules.

Remarkably, the binding mode of compound 1 shared some similarities with aspartate, which is co-crystallized with the ATP in the GatCAB structure from *Aquifex aeolicus* (PDB ID: 3H0R) (Wu et al., 2009). Tyr270 and Lys81 (*A. aeolicus* numbering) interact with aspartate through hydrogen bonding and electrostatic interaction, respectively (See Fig. S6). These two residues corresponded to Tyr271 and Lys80 in *H. pylori* GatB. Hence, the diethylphosphonate moiety of compound 1 bound to the same area as the aspartate ligand, implying that the position of the aminoacyl-adenosine, the last base of the charged tRNA in the GatB active site. In addition, the superposition of the best-docked pose of compound 1 in the *H. pylori* GatB active site and the ATP-GatB co-crystal structure of *A. aeolicus* revealed compound 1 bound to GatB with an extended conformation spanning from the ATP binding site to the area where the aminoacyl-adenosine bound (See Figs. S3 and S4). Molecular docking simulations and analyses of structural superposition suggested the binding mode of compound 1, resulting in the transamidation rate retardation observed *in vitro*. Furthermore, this binding mode was in agreement with the STD NMR data, which indicated interactions between GatB and the protons of the adenine ring, the anomeric position and the methyl group of the diethylphosphonate moiety of compound 1.

Although compound 1 exhibited inhibitory activity against *H. pylori* GatCAB *in vitro*, our *in vivo* preliminary screening for antibacterial activity indicated no growth inhibition for any of the bacteria tested (See Fig. S43 for the disc diffusion test results). The lack of *in vivo* antibacterial activity might have resulted from the poor membrane permeability of compound 1, which is relatively hydrophilic. Other studies have pointed out a similar hurdle when puromycin analogs exhibited good inhibitory activity against GatCAB *in vitro* but did not show antibacterial activity when tested against GatCAB-dependent

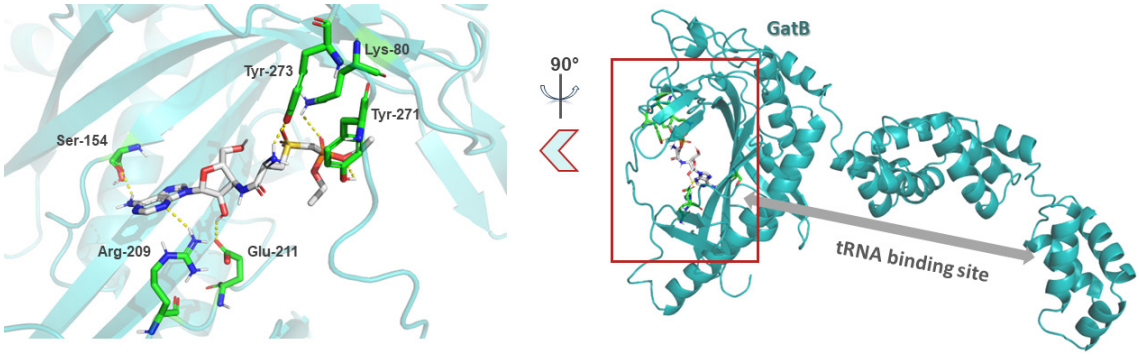

Fig. 4 Best-docked pose of compound 1 in *H. pylori* GatB model (right) and the transamidation active site with key interactions between compound 1 and GatB (left)

pathogens (Balg et al., 2008; Pham et al., 2016a). Efforts to modify the chemical structure of compound 1 to facilitate membrane permeability are ongoing by the current authors, who hope to report further discoveries in due course.

In summary, the synthesis of compound 1, a non-hydrolyzable aminoacyl-adenosine analog featuring the sulfone and diethylphosphonate groups, was accomplished starting from 3'-deoxy-3'-aminoadenosine and NHCbz-L-cysteine. This transition state mimic retarded the transamidation rate of the tRNA-dependent transamidase (GatCAB) from the human pathogen *H. pylori*. The STD NMR experiments revealed the epitope maps involved in compound 1 binding to the transamidase center in GatB. Furthermore, molecular docking simulations provided insights into the binding mode of compound 1 within the GatB active site. Nonetheless, compound 1 did not exhibit inhibitory effects on the growth of Gram-negative (*P. aeruginosa*) and Gram-positive (*S. aureus* and *B. subtilis*) bacteria. This lack of antibacterial activity was likely attributable to the hydrophilic nature of compound 1, which restricted its membrane permeability. In response, ongoing efforts by the current authors will involve structural modifications to enhance membrane penetration, with the ultimate goal of establishing the *in vivo* antibacterial activity of GatCAB inhibitors.

Conflict of Interest

The authors declare that there are no conflicts of interest.

Acknowledgements

This work was supported by the Kasetsart University Research and Development Institute (KURDI) and the Basic Research Fund (BRF) from the Faculty of Science, Kasetsart University (Grant No. BRF10/2565). The first author was supported by the Science Achievement Scholarship of Thailand (SAST). The second author was supported by the Development and Promotion of Science and Technology Talents Project (DPST). Financial support from the Center of Excellence for Innovation in Chemistry (PERCH-CIC), Ministry of Higher Education, Science, Research, and Innovation is gratefully acknowledged.

References

Agyeman, W.Y., Bisht, A., Gopinath, A., et al. 2022. A systematic review of antibiotic resistance trends and treatment options for hospital-acquired multidrug-resistant infections. Cureus 14: e29956. doi: 10.7759/cureus.29956

Aviner, R. 2020. The science of puromycin: From studies of ribosome function to applications in biotechnology. Comput. Struct. Biotechnol. J. 18: 1074–1083. doi.org/10.1016/j.csbj.2020.04.014

Balg, C., Huot, J.L., Lapointe, J., Chênevert, R. 2008. Inhibition of *helicobacter pylori* aminoacyl-tRNA amidotransferase by puromycin analogues. J. Am. Chem. Soc. 130: 3264–3265. doi.org/10.1021/ja7100714

Balg, C., Mieri, M.D., Huot, J.L., Blais, S.P., Lapointe, J., Chênevert, R. 2010. Inhibition of *Helicobacter pylori* aminoacyl-tRNA amidotransferase by chloramphenicol analogs. Bioorg. Med. Chem. 18: 7868–7872. doi.org/10.1016/j.bmc.2010.09.045

Belete, T.M. 2019. Novel targets to develop new antibacterial agents and novel alternatives to antibacterial agents. Hum. Microbiome J. 11: 100052. doi.org/10.1016/j.humic.2019.01.001

BIOVIA, D.S. 2020. Discovery Studio Visualizer, V21.1.0.20298 ed. Dassault Systèmes. San Diego, CA, USA.

Blaise, M., Bailly, M., Frechin, M., et al. 2010. Crystal structure of a transfer-ribonucleoprotein particle that promotes asparagine formation. EMBO J. 29: 3118–3129. doi.org/10.1038/emboj.2010.192

Cathopoulis, T., Chuawong, P., Hendrickson, T.L. 2007. Novel tRNA aminoacylation mechanisms. Mol. Biosyst. 3: 408–418. doi.org/10.1039/B618899K

Curnow, A.W., Hong, K.-w., Yuan, R., Kim, S.-i., Martins, O., Winkler, W., Henkin, T.M., Söll, D. 1997. Glu-tRNA^{Gln} amidotransferase: A novel heterotrimeric enzyme required for correct decoding of glutamine codons during translation. Proc. Natl. Acad. Sci. U. S. A. 94: 11819–11826. doi.org/10.1073/pnas.94.22.11819

Decicco, C.P., Nelson, D.J., Luo, Y., et al. 2001. Glutamyl-γ-boronate inhibitors of bacterial Glu-tRNA^{Gln} amidotransferase. Bioorg. Med. Chem. Lett. 11: 2561–2564. doi.org/10.1016/S0960-894X(01)00499-1

Eberhardt, J., Santos-Martins, D., Tillack, A.F., Forli, S. 2021. AutoDock Vina 1.2.0: New docking methods, expanded force field, and python bindings. J. Chem. Inf. Model. 61: 3891–3898. doi.org/10.1021/acs.jcim.1c00203

Elmaidomy, A.H., Shady, N.H., Abdeljawad, K.M., et al. 2022. Antimicrobial potentials of natural products against multidrug resistance pathogens: A comprehensive review. RSC Advances 12: 29078–29102. doi.org/10.1039/D2RA04884A

Frisch, M.J., Trucks, G., Schlegel, H.B., et al. 2009. Gaussian 09W, revision A. 02. Gaussian Inc. Wallingford, CT, USA.

Horiuchi, K.Y., Harpel, M.R., Shen, L., Luo, Y., Rogers, K.C., Copeland, R.A. 2001. Mechanistic studies of reaction coupling in Glu-tRNA^{Gln} amidotransferase. Biochemistry 40: 6450–6457. doi.org/10.1021/bi002599l

Huot, J.L., Balg, C., Jahn, D., Moser, J., Émond, A., Blais, S.P., Chênevert, R., Lapointe, J. 2007. Mechanism of a GatCAB amidotransferase: Aspartyl-tRNA synthetase increases its affinity for Asp-tRNA^{Asn} and novel aminoacyl-tRNA analogues are competitive inhibitors. Biochemistry 46: 13190–13198. doi.org/10.1021/bi700602n

Ibba, M., Söll, D. 2000. Aminoacyl-tRNA synthesis. Annu. Rev. Biochem. 69: 617–650. doi.org/10.1146/annurev.biochem.69.1.617

Igonet, S., Raingeval, C., Cecon, E., et al. 2018. Enabling STD-NMR fragment screening using stabilized native GPCR: A case study of adenosine receptor. Sci. Rep. 8: 8142. doi.org/10.1038/s41598-018-26113-0

Khuntong, S., Sudprasert, W. 2008. Extraction and basic testing for antibacterial activity of the chemical constituents in *Suregada multiflorum*. Kasetsart J. (Nat. Sci.) 42: 429–434.

Klinchan, C., Hsu, Y.-L., Lo, L.-C., Pluempanupat, W., Chuawong, P. 2014. Synthesis of non-hydrolyzable substrate analogs for Asp-tRNA^{Asn}/Glu-tRNA^{Gln} amidotransferase. Tetrahedron Lett. 55: 6204–6207. doi.org/10.1016/j.tetlet.2014.09.060

Lin, J., Zhou, D., Steitz, T.A., Polikanov, Y.S., Gagnon, M.G. 2018. Ribosome-targeting antibiotics: Modes of action, mechanisms of resistance, and implications for drug design. Annu. Rev. Biochem. 87: 451–478. doi.org/10.1146/annurev-biochem-062917-011942

Meyer, B., Peters, T. 2003. NMR spectroscopy techniques for screening and identifying ligand binding to protein receptors. Angew. Chem. Int. Ed. 42: 864–890. doi.org/10.1002/anie.200390233

Nakamura, A., Sheppard, K., Yamane, J., Yao, M., Soll, D., Tanaka, I. 2010. Two distinct regions in *Staphylococcus aureus* GatCAB guarantee accurate tRNA recognition. Nucleic Acids Res. 38: 672–682. doi.org/10.1093/nar/gkp955

Nakamura, A., Yao, M., Chimnaronk, S., Sakai, N., Tanaka, I. 2006. Ammonia channel couples glutaminase with transamidase reactions in GatCAB. Science 312: 1954–1958. doi: 10.1126/science.1127156

Namsena, P., Maneetap, J., Phonpheng, D., Ngamsane, W. 2019. Comparative study of antibacterial activity and phytochemical analysis of stem, root and leaf extracts of *Paederia foetida* L. against phytopathogenic bacteria. Agr. Nat. Resour. 53: 395–401. doi.org/10.34044/j.anres.2019.53.4.10

Pham, V.H., Lapointe, J. 2017. The bacterial heterotrimeric amidotransferase GatCAB: functions, structures and mechanism-based inhibitors. Arch. Biotechnol. Biomed. 1: 21–32. doi: 10.29328/journal.hjb.1001003

Pham, V.H., Maaroufi, H., Balg, C., et al. 2016. Inhibition of *Helicobacter pylori* Glu-tRNA^{Gln} amidotransferase by novel analogues of the putative transamidation intermediate. FEBS Lett. 590: 3335–3345. doi.org/10.1002/1873-3468.12380

Pham, V.H., Maaroufi, H., Levesque, R.C., Lapointe, J. 2016. Cyclic peptides identified by phage display are competitive inhibitors of the tRNA-dependent amidotransferase of *Helicobacter pylori*. Peptides 79: 8–15. doi.org/10.1016/j.peptides.2016.03.001

Rathnayake, U.M., Wood, W.N., Hendrickson, T.L. 2017. Indirect tRNA aminoacylation during accurate translation and phenotypic mistranslation. Curr. Opin. Chem. Biol. 41: 114–122. doi.org/10.1016/j.cbpa.2017.10.009

Romeo, R., Carnovale, C., Giofrè, S.V., et al. 2012. Truncated phosphonated C-1′-branched N,O-nucleosides: A new class of antiviral agents. Bioorg. Med. Chem. 20: 3652–3657. doi.org/10.1016/j.bmc.2012.03.047

Rossiter, S.E., Fletcher, M.H., Wuest, W.M. 2017. Natural products as platforms to overcome antibiotic resistance. Chem. Rev. 117: 12415–12474. doi.org/10.1021/acs.chemrev.7b00283

Sae-lim, S., Puttamuk, T., Maneeanakekul, S., Buppatano, S., Pluempanupat, W., Chuawong, P. 2023. *Morinda scabrida* Craib: An unexplored species with antibacterial potential and inhibition of acetylcholine esterase and α-glucosidase. Agr. Nat. Resour. 57: 729–738. doi.org/10.34044/j.anres.2023.57.4.17

Sanner, M.F. 1999. Python: A programming language for software integration and development. J. Mol. Graph. Model. 17: 57–61.

Schrödinger, L. 2023. The PyMOL Molecular Graphics System, Version 2.5.5. Schrödinger. San Diego, CA, USA.

Suzuki, T., Nakamura, A., Kato, K., Soll, D., Tanaka, I., Sheppard, K., Yao, M. 2015. Structure of the *Pseudomonas aeruginosa* transamidosome reveals unique aspects of bacterial tRNA-dependent asparagine biosynthesis. Proc. Natl. Acad. Sci. U.S.A. 112: 382–387. doi.org/10.1073/pnas.1423314112

Trott, O., Olson, A.J. 2010. AutoDock Vina: Improving the speed and accuracy of docking with a new scoring function, efficient optimization, and multithreading. J. Comput. Chem. 31: 455–461. doi.org/10.1002/jcc.21334

Veyron, B., Picq, D., Anker, D. 1989. Et_3N, 3HF, a new fluorinating reagent. Some evidence for the existence of Et_3N, 2HF. J. Fluor. Chem. 45: 130. doi.org/10.1016/S0022-1139(00)84502-9

Vila, J., Moreno-Morales, J., Ballesté-Delpierre, C. 2020. Current landscape in the discovery of novel antibacterial agents. Clin. Microbiol. Infect. 26: 596–603. doi.org/10.1016/j.cmi.2019.09.015

Woese, C.R., Olsen, G.J., Ibba, M., Soll, D. 2000. Aminoacyl-tRNA synthetases, the genetic code, and the evolutionary process. Microbiol. Mol. Biol. Rev. 64: 202–236. doi.org/10.1128/mmbr.64.1.202-236.2000

Wu, J., Bu, W., Sheppard, K., Kitabatake, M., Kwon, S.T., Soll, D., Smith, J.L. 2009. Insights into tRNA-dependent amidotransferase evolution and catalysis from the structure of the Aquifex aeolicus enzyme. J. Mol. Biol. 391: 703–716. doi.org/10.1016/j.jmb.2009.06.014

Yang, J., Zhang, Y. 2015. I-TASSER server: New development for protein structure and function predictions. Nucleic Acids Res. 43: W174–W181. doi.org/10.1093/nar/gkv342

Zhao, L., Dewage, S.W., Bell, M.J., et al. 2012. The kinase activity of the *Helicobacter pylori* Asp-tRNA^{Asn}/Glu-tRNA^{Gln} amidotransferase is sensitive to distal mutations in its putative ammonia tunnel. Biochemistry 51: 273–285. doi.org/10.1021/bi201143x

Zhao, L., Rathnayake, U.M., Dewage, S.W., Wood, W.N., Veltri, A.J., Cisneros, G.A., Hendrickson, T.L. 2016. Characterization of tunnel mutants reveals a catalytic step in ammonia delivery by an aminoacyl-tRNA amidotransferase. FEBS Lett. 590: 3122–3132. doi.org/10.1002/1873-3468.12347

Zheng, W., Zhang, C., Li, Y., Pearce, R., Bell, E.W., Zhang, Y. 2021. Folding non-homologous proteins by coupling deep-learning contact maps with I-TASSER assembly simulations. Cell Rep. Methods 1: 100014. doi.org/10.1016/j.crmeth.2021.100014

Zhou, X., Zheng, W., Li, Y., Pearce, R., Zhang, C., Bell, E.W., Zhang, G., Zhang, Y. 2022. I-TASSER-MTD: A deep-learning-based platform for multi-domain protein structure and function prediction. Nat. Protoc. 17: 2326–2353. doi.org/10.1038/s41596-022-00728-0